Available online at www.sciencedirect.com
ScienceDirect
Journal of Photochemistry and Photobiology A: Chemistry 192 (2007) 8–16
Journal of Photochemistry and Photobiology A:Chemistry
www.elsevier.com/locate/jphotochem

Bisindolylmaleimide derivatives as non-doped red organic light-emitting materials

Zhijun Ning [a], Yechun Zhou [b], Qiong Zhang [a], Dongge Ma [c], Junji Zhang [a], He Tian [a,*]

[a] *Laboratory for Advanced Materials and Institute of Fine Chemicals, East China University of Science and Technology, Meilong Road, Shanghai 200237, China*
[b] *State Key Laboratory of Surface Physics, Fudan University, Shanghai 200433, China*
[c] *State Key Laboratory of Polymer Physics and Chemistry, Changchun Institute of Applied Chemistry, Chinese Academy of Sciences, Changchun 130022, China*

Received 24 January 2007; received in revised form 19 March 2007; accepted 30 April 2007
Available online 3 May 2007

Abstract

A new series of bisindolylmaleimide (BIM) derivatives were synthesized. The absorption and fluorescence properties of these compounds were investigated in solution and solid state. Dramatic difference in solid-state fluorescence emission spectra was observed by changing the substituents on the fluorophores skeleton from methyl to benzyl. We performed X-ray crystallographic analyses to elucidate the effect of the substituents of the non-conjugated linkage on the solid-state fluorescence emission spectra. The relationships between the solid-state photophysical properties and the chemical and crystal structures of 2,3-bis(*N*-benzyl-2′methyl-3′-indolyl)-*N*-methylmaleimide (**1S**) and 2,3-bis(*N*-benzyl-2′methyl-3′-indolyl)-*N*-benzylmaleimide (**5S**) are discussed on the basis of the X-ray crystal data. Bis[2,3-bis(*N*-ethyl-2′methyl-3′-indolyl)-*N*-(prop-2-ynyl)maleimide] (**1B**) and **1S** were utilized in non-doping host red EL device. The brightness reaches 393 cd m^{-2} at 100 mA cm^{-2} for **1S**.

Keywords: Non-doped red organic light-emitting diodes; Bis-indolylmethylmaleimide; Fluorescence; Crystal structures; Substituent effects

1. Introduction

Organic fluorophores with strong solid-state emission have attracted increasing interest for their important use in the fundamental research field of solid-state photochemistry [1–4] and in the applied field of optoelectronic devices [5–8]. However, organic fluorophores with high solid-state emission are less common. Many organic chromophores are highly emissive in dilute solutions but become weakly luminescent or non-luminescent in their solid states. The aggregation caused by the strong intermolecular π–π interaction [9–11] or intermolecular hydrogen bonding [12], between neighboring fluorophores in solid state, generally debases or quenches the emission. Much effort had been made to change fluorophores from weakly luminescent to strongly emissive in solid state, such as the introduction of bulky substituents onto the original fluorophores, and the formation of clathrates or salts with fluorophores [13–17]. However, generally, the solid-state properties of molecular aggregates are the result of the interplay of different subtle factors which are difficult to separate and identify [18–20]. Even a slight structural modification of a given molecule may have a great effect on its fluorescence in solid state [21]. By far, there still lack well-established guidance approaches for enhancing luminescence in solid state.

For most fluorophores, the configuration is planar or approximately planar for conjugation. The planar configuration will inevitably bring about aggregation, and then debase fluorescence. This becomes more serious when the emission wavelength is bathochromic shifted to red region, for it is generally required to extend the molecule dimension which will aggravate aggregation [22]. Due to the difficulty in enlarging the molecule dimension while keeping the neighboring molecules from aggregation in solid state, up to now red fluorophores with high emission in solid state were especially few. This brought huge difficulty in the manufacture of red organic light-emitting diodes (OLED), for fluorophores were

* Corresponding author. Tel.: +86 21 64252288; fax: +86 21 64252288.
E-mail address: tianhe@ecust.edu.cn (H. Tian).

1010-6030/$ – see front matter © 2007 Elsevier B.V. All rights reserved.
doi:10.1016/j.jphotochem.2007.04.030

thus required to be doped into host materials, yet dopant emitters are difficult to adapt for mass production [23,24]. It is urgent to develop red fluorophores which are highly emissive in solid state and can be applied in OLED. Some red fluorophores such as *N*-methyl-bis(4-(*N*-(1-naphthyl)-*N*-phenylamino)phenyl)maleimide (NPAMLMe) and 2,3-dicyano-5,6-(4′-diphenylamino-biphenyl-4-yl)-pyrazine (CAPP) had been synthesized and applied in emitting-host non-doped red OLED [25–30]. Bisindolylmaleimides (BIM) derivatives were firstly applied in OLED [31,32]. We noticed that some of the red fluorophores have similar configuration, so maybe some of them have a common special cumulate pattern in solid state which can inhibit the aggregation effectively.

In this work, we synthesized a new series of bisindolylmaleimides (BIM) derivatives, whose solid-state fluorescence can be dramatically changed by introduction of different substituents on the non-conjugated linkage to the BIM skeleton. We carried out X-ray crystallographic analyses of compounds **1S** and **5S** to elucidate the relationship between the photophysical properties and the chemical and crystal structures. Two dyes were preliminarily fabricated into emitting-host non-doped red OLED.

2. Experiment

^{1}H NMR spectra were obtained using a Brüker AM 500 spectrometer (relative to TMS). Mass spectra were done with a HP5989 mass spectrometer, and UV–vis spectra on a Varian Cary 500 spectrophotometer. Fluorescence emission spectra were recorded on a Varian Cary Eclipse fluorescence spectrophotometer. Luminescence lifetime measurements were performed on an Edinburgh FL 900. Glass transition temperatures (T_g) were measured using PerkinElmer Pyris Diamond TG/DTA instrument at a scan rate of 20 °C min^{-1}. Cyclic voltammetry was performed using an Potentiostat/Galvanostat Model K0264 (Princeton Applied Research). Anhydrous CH_2Cl_2 was used as the solvent under inert atmosphere, and 0.1 M tetra(*n*-butyl)ammonium perchlorate was used as the supporting electrolyte. A platinum disk electrode was used as the working electrode; a platinum wire was used as the counter electrode, and a saturated Ag/AgCl reference electrode.

2.1. General procedure for synthesizing bisindolylmaleimides derivatives

The intermediate bis-2-methylindolylmaleimide was prepared according to known procedures [31]. *N*-Alkylation was done by first deprotonation of bis-indolylmaleimide (1 mmol) in DMF (5 mL) with NaH (1 mmol). To the mixture was added alkyl bromide reactant 1.1 mmol or 4 mmol dropwise, then it was stirred with a magnetic bar at room temperature for 3 h. The reaction was quenched by the addition of water, and was filtered. The filtrate was purified through silica gel column chromatograph eluted with CH_2Cl_2/hexane.

2.1.1. Compound ***1B***: *bis[2,3-bis(N-ethyl-2′methyl-3′-indolyl)-N-(prop-2-ynyl)maleimide]*

Yield 70%, 2,3-bis(*N*-diethyl-2′methyl-3′-indolyl)-*N*-(prop-2-ynyl)maleimide (0.1 g, 0.22 mmol) was dissolved in THF. $Pd(PPh_3)_2Cl_2$ (7.8 mg, 0.011 mmol), CuI (2.0 mg, 0.011 mmol) and I_2 (2.8 mg, 0.011 mmol) were then added. The mixture was stirred with a magnetic bar at room temperature for 3 h. The solvent was dried in vacuo. The crude product was purified through silica gel column chromatograph eluted with ethyl acetate/CH_2Cl_2. ^{1}H NMR ($CDCl_3$)—*δ*: 1.17 (t, 12H), 1.97 (s, 12H), 4.11 (q, 8H, *J* = 7.0 Hz), 4.55 (s, 4H), 6.89 (br, 4H), 7.08 (t, 8H, *J* = 7.3 Hz), 7.21 (d, 4H, *J* = 8.1 Hz), MS (ESI), *m/e*: 919.3 (100%) [M + Na$^+$].

2.1.2. Compound ***2B***: *bis[2,3-bis(N-dodecyl-2′methyl-3′-indolyl)-N-(prop-2-ynyl)maleimide]*

Yield 68%, the preparation of **2B** was similar to that of **1B**. ^{1}H NMR ($CDCl_3$)—*δ*: 0.88 (t, 12H), 1.97 (s, 12H), 4.11 (q, 8H, *J* = 7.0 Hz), 4.55 (s, 4H), 6.89 (br, 4H), 7.08 (t, 8H, *J* = 7.3 Hz), 7.21 (d, 4H, *J* = 8.1 Hz), MS (ESI), *m/e*: 1457.6 (100%) [M + 1$^+$].

2.1.3. Compound ***1S***: *2,3-bis(N-benzyl-2′methyl-3′-indolyl)-N-methylmaleimide*

Yield 55%, ^{1}H NMR ($CDCl_3$)—δ: 2.04 (br, 6H), 3.22 (s, 3H), 4.74 (br, 4H), 6.69 (br, 2H), 6.93 (br, 4H), 7.01–7.24 (br, 12H), MS (EI), *m/e*: 549 (100%) [M$^+$].

2.1.4. Compound ***2S***: *2,3-bis[N-4(cyano)benzyl-2′methyl-3′-indolyl]-N-methylmaleimide*

Yield 73%, ^{1}H NMR ($CDCl_3$)—*δ*: 2.02 (br, 6H), 3.24 (s, 3H), 5.13 (br, 4H), 6.76 (br, 2H), 6.80–7.24 (br, 10H), 7.28–7.63 (br, 4H), MS (EI), *m/e*: 599 (100%) [M$^+$].

2.1.5. Compound ***3S***: *2,3-bis{N-[4-(5-phenyl)-1,3,4-oxadiazoly]benzyl-2′methyl-3′-indolyl}-N-methylmaleimide*

Yield 75%, ^{1}H NMR ($CDCl_3$)—*δ*: 2.07 (s, 6H), 3.25 (s, 3H), 5.14–5.42 (br, 4H), 6.78 (br, 2H), 7.01 (br, 4H), 7.06–7.24 (br, 4H), 7.25(br, 2H), 7.45–7.56 (br, 6H), 7.71–7.97 (br, 4H), 8.05 (d, 4H, *J* = 6.9 Hz), MS (EI), *m/e*: 837 (100%) [M$^+$].

2.1.6. Compound ***4S***: *2,3-bis(N-benzyl-2′methyl-3′-indolyl)-N-4(cyano)benzylmaleimide*

Yield 73%, ^{1}H NMR ($CDCl_3$)—*δ*: 2.01 (br, 6H), 4.92 (s, 2H), 5.12 (br, 4H), 6.62–6.98 (br, 6H), 7.02–7.24 (br, 12H), 7.61 (d, 2H, *J* = 8.2 Hz), 7.66 (d, 2H, *J* = 8.2 Hz), MS (EI), *m/e*: 655 (36.98%) [M$^+$].

2.1.7. Compound ***5S***: *2,3-bis(N-benzyl-2′methyl-3′-indolyl)-N-benzylmaleimide*

Yield 85%, ^{1}H NMR ($CDCl_3$)—*δ*: 2.01 (br, 6H), 4.88 (s, 2H), 5.26 (br, 4H), 6.63–6.99 (br, 6H), 7.03–7.23 (br, 12H), 7.31 (t, 1H, *J* = 7.4 Hz), 7.35 (t, 2H, *J* = 7.2 Hz), 7.53 (d, 2H, *J* = 7.3 Hz), MS (EI), *m/e*: 625 (57.30%) [M$^+$].

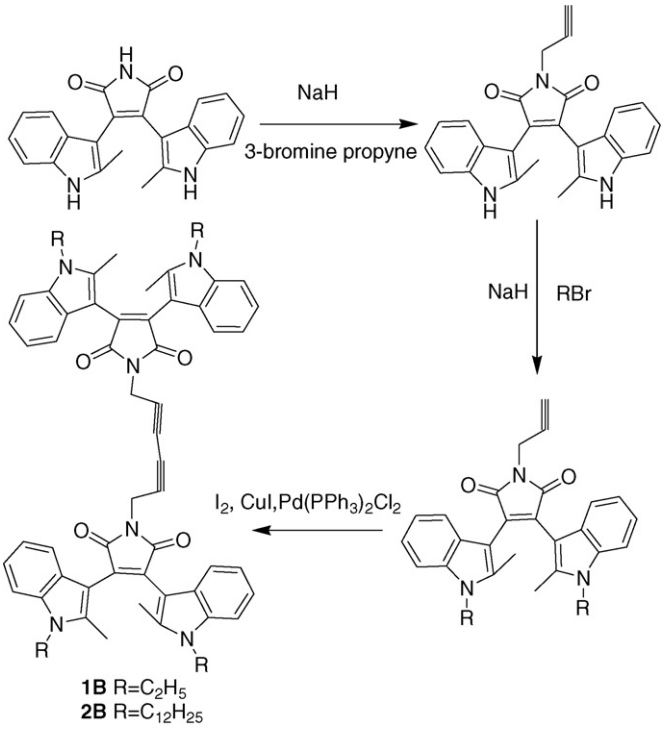

Scheme 1. Synthetic route of compounds **1B** and **2B**.

*2.1.8. Compound **6S**: 2,3-bis(2′,N-dimethyl-3′-indolyl)-N-methylmaleimide*

Yield 75%, ^{1}H NMR ($CDCl_3$)—δ: 2.03 (s, 6H), 3.21 (s, 3H), 3.59 (s, 6H), 6.92 (br, 2H), 7.11 (t, 4H, J = 7.3 Hz), 7.21 (d, 2H, J = 8.1 Hz) MS (EI), *m/e*: 397 (100%) [M^+].

2.2. OLED device fabrication and characterization

The device is fabricated on indium tin oxide (ITO) coated glass plate which is cleaned by routine procedure including ultrasonication in detergent and de-ionized water sequentially and a final UV ozone treatment. In a vacuum chamber at a pressure of $<8 \times 10^{-5}$ Pa, 50 nm of NPB as the hole transporting layer, 10 nm of the BIM derivatives as the emitting layer, 50 nm of TPBI as the electron transporting layer, and a LiF (0.7 nm)/Al (100 nm) bilayer as cathode. The current–voltage (*I–V*) profiles and light intensity characteristics for the above

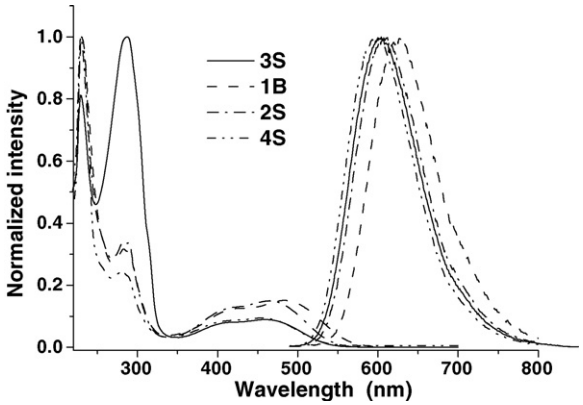

Fig. 1. Normalized absorption (left) and emission (right) spectra of **1B**, **2S**, **3S** and **4S** in solution.

fabricated devices were measured in atmosphere at ambient temperature. The electroluminescence (EL) spectra were measured with a Spectra Scan PR705. The current–voltage (*I–V*) and luminance–voltage (*L–V*) characteristics were measured with a Keithley236 source unit and Keithley 2000-20 with ST-86LA luminance meter.

3. Results and discussion

The synthesis of the target products is depicted in Schemes 1 and 2. Because of the different reactive activity between the hydrogen atoms on maleimide and indole, *N*-alkylation can be selectively done firstly on the imine of maleimide, and then on the imine of the indoles by cautious control of the dosage of alkyl bromide.

The absorption and emission spectra of the compounds were investigated in dichloromethane and dioxane solutions. The absorption and luminescence data of the compounds are presented in Table 1. Representative absorption and emission spectra are shown in Figs. 1 and 2. The absorption and emission wavelengths exhibit a moderate solvatochromism, which was evidenced by the red shift of the fluorescence maxima in the dichloromethane compared to that in dioxane. The fluorescence properties are significantly dependent on the solvent polarity. The fluorescence (FL) quantum yield is reduced significantly by changing the solvent from dioxane to dichloromethane. Similar

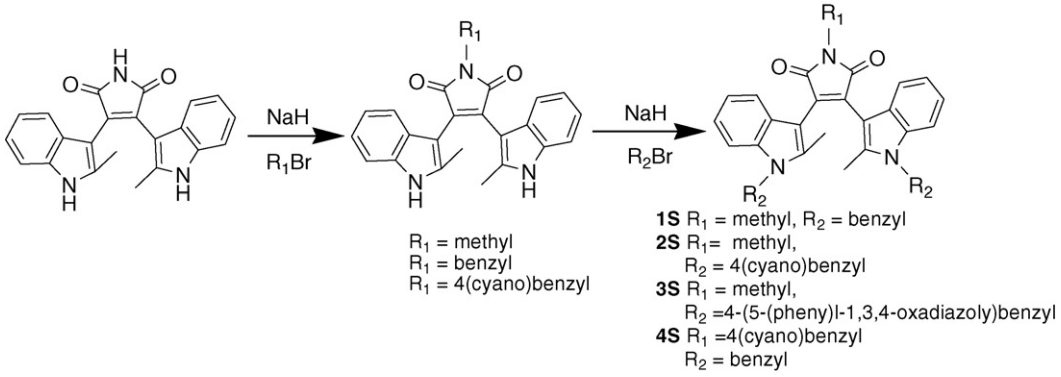

Scheme 2. Synthetic route of compounds **1S–4S**.

Table 1
Summary of the photophysical and electrochemical property of **1B**, **2B**, **1S**–**5S**

Compounds	1B	2B	1S	2S	3S	4S	5S
λ_{max} (nm), CH_2Cl_2	482	485	464	452	459	476	461
λ_{em} (nm), 1,4-dioxane	595	593	580	575	579	591	582
Φ (%), 1,4-dioxane	22.5	21.4	47.5	58.0	58.6	38.4	47.0
λ_{em} (nm), CH_2Cl_2	623	622	606	598	604	617	605
Φ (%), CH_2Cl_2	3.7	3.1	15.0	27.1	19.0	10.8	16.5
λ_{em} (nm), solid state	631	630	609	617	626	608	617
HOMO (eV)	−5.40	−5.39	−5.45	−5.49	−5.49	−5.48	−5.37
LUMO (eV)	−3.12	−3.13	−3.08	−3.03	−3.03	−3.05	−3.06

spectral changes were generally observed for most fluorescent dyes whose dipole moments in the excited state are larger than those in the ground state [33]. Compounds **1S**, **2S**, **3S**, **4S** and **5S** (Scheme 3) have almost the same FL quantum yields in solution. However, the FL quantum yields of **1B** and **2B** are relatively lower in solution due to their weaker molecular rigidity compared with others.

Interesting results have been obtained for the photophysical properties of microcrystal powders of **1S**, **5S** and **6S**. Fig. 3 shows that the fluorescence intensity of **1S**, **5S** and **6S** are quite different in solid state. Compound **1S** exhibits strong fluorescence, while **6S** is nearly non-luminescecent in solid state. The fluorescence intensity of **1S** was nearly eight-fold larger than that of **5S**, and compounds **2S**, **3S**, **4S** and **5S** have almost the same fluorescence intensity in solid state. We also examined the fluorescence lifetime for **1S** and **5S** in solid state (Table 2). The fluorescence lifetime of **1S** (8.09 ns) is consumedly longer than that of **5S** (3.25 ns), which is in accordance with their fluorescence intensity in solid state.

To understand the dramatic substituent effect on the solid-state photophysical properties, the X-ray crystal structures of compounds **1S** and **5S** were determined and are shown in Fig. 4. Crystal parameters and refinement data are listed in Table 3. It is clear that the two indole rings are not coplanar with the ring of maleimide. Rotation across the inner bay region is restricted by steric hindrance between the methyl groups at C4 and C4′. Two dihedral angles between indole rings and maleimide ring were both 53.17° for **1S**, while 42.27° and 48.91° for **5S**, respectively. It can be seen obviously in Fig. 4 that the dramatic difference between the crystal conformations of **1S** and **5S** is that two indole rings are parallel for **5S** but antiparallel for **1S**.

The dihedral angles between the two indole rings of **1S** is 77.38° which is about 20 degrees larger than that of **5S** (Table 4). The dihedral angles between two indole rings and malemide ring of **1S** are both larger than those of **5S**. By comparison of the three

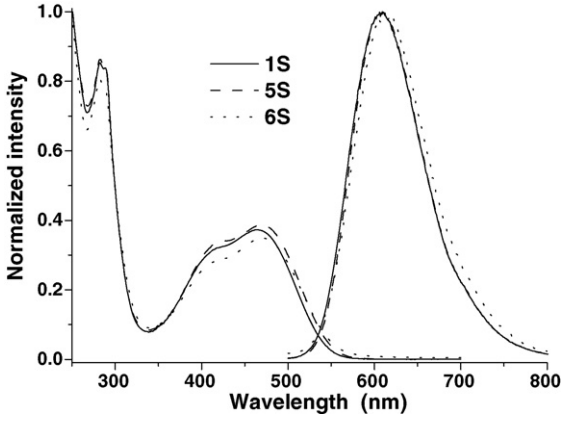

Fig. 2. Normalized absorption (left) and emission (right) spectra of **1S**, **5S** and **6S** in solution.

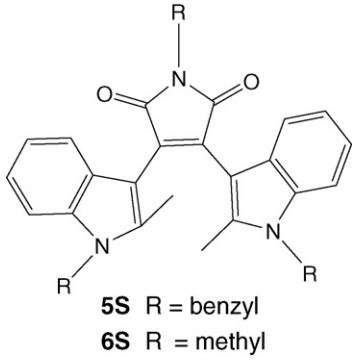

Scheme 3. Molecular structures of **5S** and **6S**.

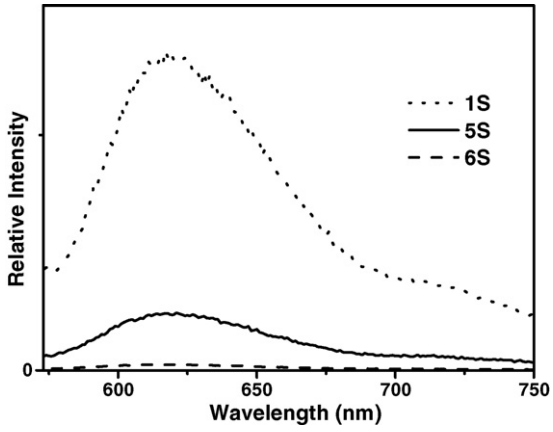

Fig. 3. Photoluminescence spectra of **1S**, **5S** and **6S** in solid state.

Table 2
Luminescence lifetime and glass transition temperature (T_g) of **1S** and **5S** in solid state

Compound	τ (ns)	χ^2	T_g (°C)
1S	8.09	1.056	176
5S	3.25	1.012	98

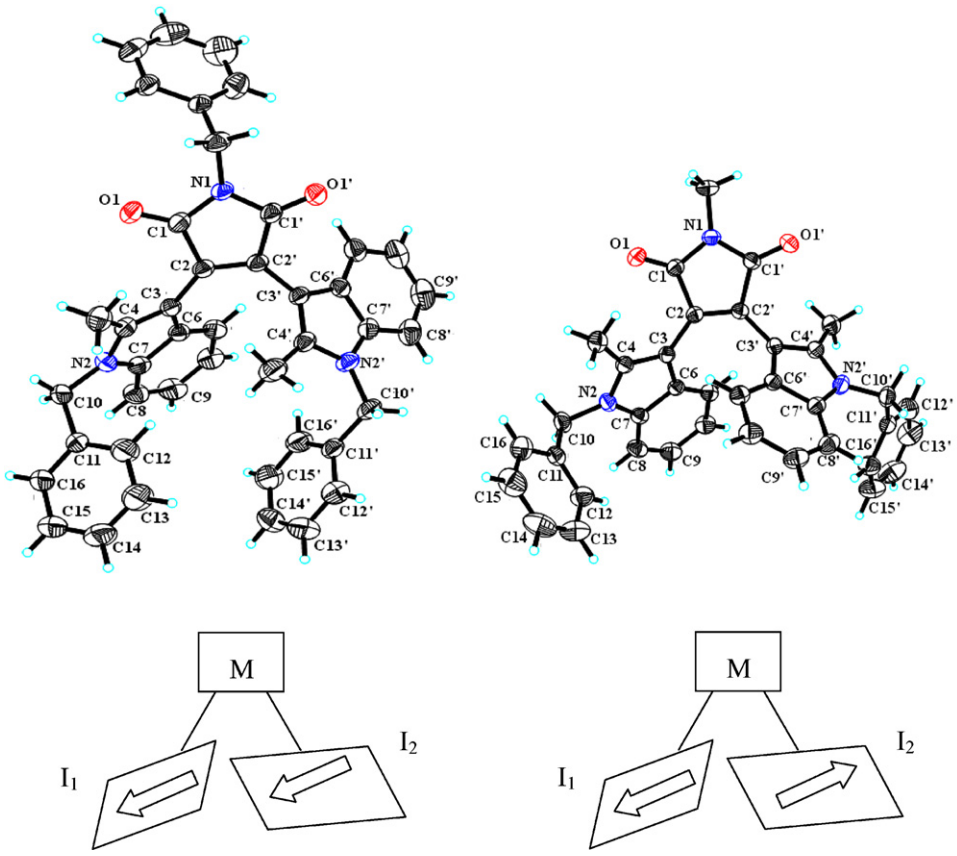

Fig. 4. X-ray-determined molecule structures of **5S** (left) and **1S** (right). The sketches below each diagram depict the molecular structures. The arrows in the above sketches indicate the direction from the benzene ring to pyrrole ring in indole substituent.

privotal dihedral angels in the fluorophore skeleton, we can see that the non-coplanarity of **1S** is considerably better than **5S**. In compound **1S** the indole planes are nearly perpendicular to the benzyl planes locating on the indole moiety. The molecular configuration of **1S** in crystal seems like a "pyramid". The maleimide is the peak of the tower, the two indole rings are the side face and the two benzyl rings are the underside. This kind of non-planar conformation tends to inhibit aggregation effectively

Table 3
Summary of crystal data collection and structure refinement of compounds **1S**, **5S** and **6S**

Compound	**1S**	**5S**	**6S** [8]
Empirical formula	$C_{37}H_{31}N_3O_2$	$C_{43}H_{35}N_3O_2$	$C_{25}H_{23}N_3O_2$
Formula weight	549.65	625.74	397.46
Temperature (K)	293(2)	293(2)	293(2)
Wavelength (Å)	0.71073 (Mo Kα)	0.71073 (Mo Kα)	0.71073 (Mo Kα)
Crystal system monoclinic	Monoclinic	Monoclinic	Triclinic
Space group	*P*2/*n*	*P*2(1)/*n*	*P*-1
a (Å)	10.3506(11)	9.2656(9)	8.344(3)
b (Å)	9.0689(9)	15.9306(16)	10.043(3)
c (Å)	15.2872(16)	22.717(2)	12.731(4)
α (°)	90	90	82.65(3)
β (°)	91.405(2)	90.283(2)	88.36(3)
γ (°)	90	90	74.72(2)
Z	2	4	2
D_{calcd} (Mg m^{-3})	1.272	1.240	1.293
F(0 0 0)	580	1320	420
Crystal size (mm)	0.508 × 0.436 × 0.313	0.467 × 0.193 × 0.161	0.4 × 0.32 × 0.15
θ range	2.25–26.99	1.56–26.00	1.61–24.98
GOF	0.823	0.865	1.044
R^b indices [$I > 2\sigma(I)$]	$R1 = 0.0429$, $wR2 = 0.0993$	$R1 = 0.0462$, $wR2 = 0.1168$	$R1 = 0.0597$, $wR2 = 0.1699$
R^b indices (all data)	$R1 = 0.0818$, $wR2 = 0.0993$	$R1 = 0.0462$, $wR2 = 0.1168$	$R1 = 0.1234$, $wR2 = 0.2097$
Largest diff. peak and hole	0.148 and −0.129	0.133 and −0.144	0.337 and −0.353

Table 4
Selected bond lengths and dihedral angles of the crystal structures of compounds **1S**, **5S** and **6S**

Structural parameters	Compound **1S**	Compound **5S**	Compound **6S** [8]
C2–C2′ (Å)	1.345(3)	1.352(3)	1.351(4)
C2–C3 (Å)	1.457(2)	1.452(3)	1.448(4)
C2′–C3′ (Å)	1.457(2)	1.460(3)	1.461(4)
C2′–C2–C3 (°)	130.2(8)	130.1(2)	131.4(3)
C1–C2–C3 (°)	121.3(13)	122.2(2)	121.1(3)
C2–C2′–C3′ (°)	130.2(8)	130.4(2)	130.5(3)
Cl′–C2′–C3′ (°)	121.3(13)	121.1(2)	121.4(3)
N1–C1–C2–C1′–C2′ and N2–C3–C4–C6–C8–C7–C9 (°)	53.17	42.27	36
N1–C1–C2–C1′–C2′ and N2′–C3′–C4′–C6′–C8′–C7′–C9′ (°)	53.17	48.91	40
N2–C3–C4–C6–C8–C7–C9 and N2′–C3′–C4′–C6′–C8′–C7′–C9′ (°)	77.38	59.51	–
N2–C3–C4–C6–C8–C7–C9 and C11–C12–C13–C14–C15 (°)	69.72	88.38	–
N2′–C3′–C4′–C6′–C8′–C7′–C9′ and Cll′–C12′–C13′–C14′–C15′ (°)	69.92	83.64	–

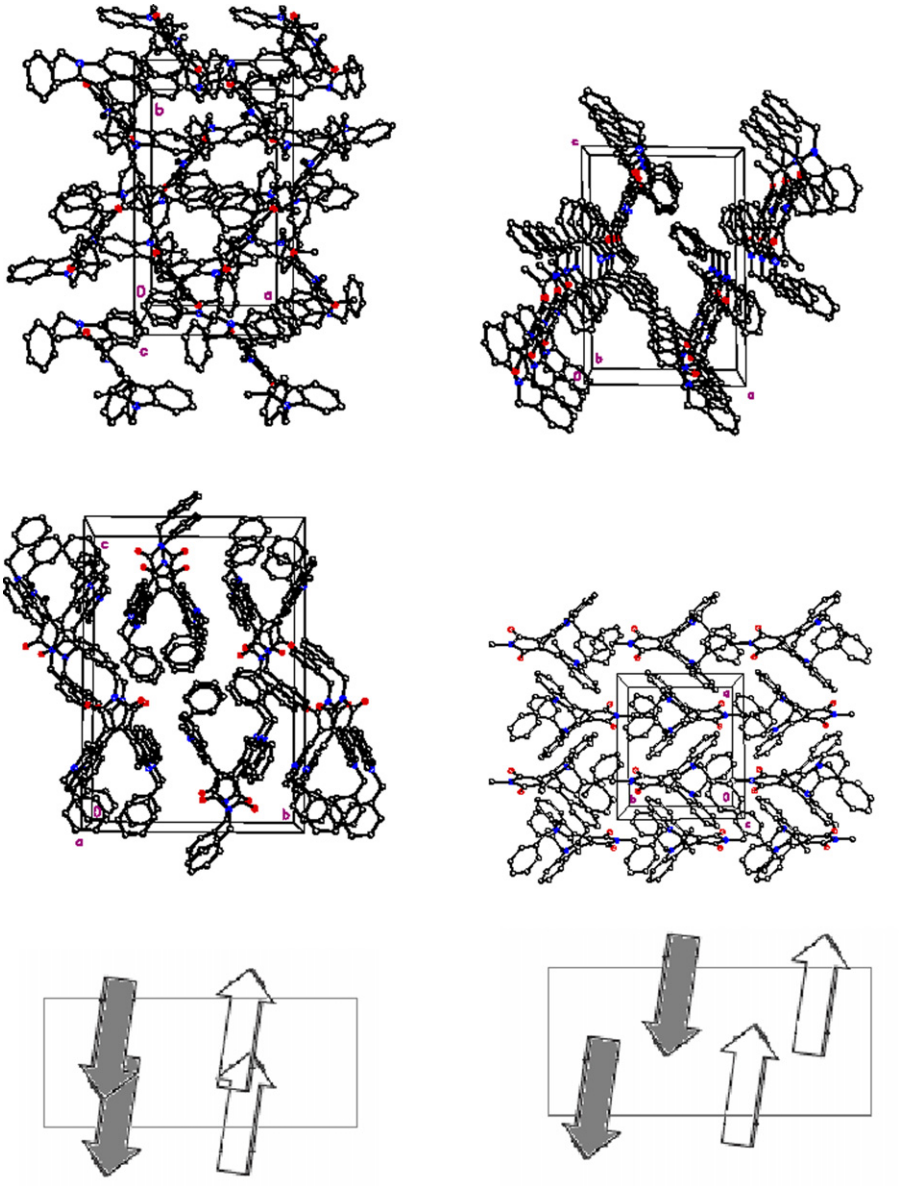

Fig. 5. Crystal-packing diagrams of **5S** (left) and **1S** (right), all the hydrogen had been removed for clarity. The sketches below each diagram depict the crystal packing in the unit cell of **5S** and **1S**. The arrows in the below sketches indicate direction from indole-to-maleimide substituent.

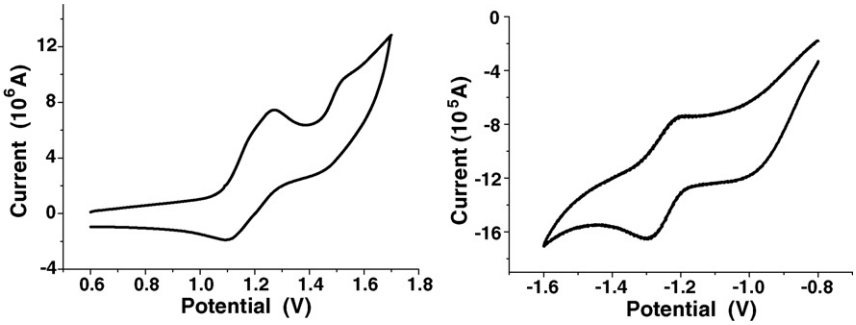

Fig. 6. Oxidative (left) and reductive (right) cyclic voltammetry plots of compound **4S**, measured in dichloromethane.

[34]. For **5S**, its non-coplanarity is not as good as **1S** and it still tends to favor H-aggregation. We can see the difference clearly in Fig. 5. As a consequence the FL intensity of **1S** is considerably higher than that of **5S** in solid state. The single crystal of **6S** also had been reported [31], the two indole rings of which were parallel as **5S**. However, the lack of the two benzyl substitutents makes it easier to aggregate, and the fluorescence intensity of **6S** is lower than that of **5S** in solid state. We notice that some non-dopant type red emitting materials like NPAMLMe and CAPP also have the similar structure with **1S**, in which an electron-accepting group locating on the upside and two electron-donor substituents on the downside [24,28]. With this kind of configuration, the molecule dimension was enlarged enough to emit red light, and high emission was kept in solid state simultaneously, making them promising candidates for emitting-host non-doped red OLED.

On the other hand, the glass transition temperature (T_g) of **1S** is 176 °C consumedly higher than that of **5S** (98 °C). By calculating the molecular volumes based on crystallographic data, the two molecular volumes of them were got, they are 717 Å for **1S** and 838 Å for **5S**. Considering they have similar molecular structures and volumes, we speculate that the different molecular accumulation pattern is the primary causation for the huge difference in T_g [34]. It is likely that the "pyramid-mimetic" structure can reduce the contact between molecules effectively, and then enhance the T_g, which is an important parameter for OLED emitting materials.

Another interesting phenomenon is why the FL quantum yields of **1S** and **5S** in solution are approximately the same while differ so much in solid state. We noticed that the BIM have the similar molecule conformation with diarylethene, which was one of the most promising photochromic compounds [35]. It has been confirmed that the diarylethene compound have about equal amount of antiparallel and parallel conformation molecules in solution. So we speculate that, for the BIM derivatives, there are also about equal amount of antiparallel and parallel conformation molecules in solution so that **1S** and **5S** have close FL quantum yields in solution. But in crystal state, only one conformation exist either parallel or antiparallel [36], which brings about the huge difference in accumulation pattern in solid state. It has been confirmed that the photocyclization reaction of diarylethene can proceed only in antiparallel conformation in crystal state [37]. In view of the similar structure of BIM and diarylethene, maybe we can get some elicitation for the molecule design of diarylethene compounds with antiparallel configuration in crystal state.

Oxidation potentials of these compounds were measured by cyclic voltammetry (CV) in dichloromethane using Ag/AgCl as a reference electrode. Each compound of **1B**, **2B** and **1S**–**5S** showed one or two pairs of reversible redox peaks such as **4S** (Fig. 6). The reversible nature of these peaks indicates the electrochemical stability of these compounds. The half-peak potentials ($E_{1/2} = 1/2(E_{pa} + E_{pc})$) of the first oxidation waves were estimated to be 1.09, 1.08, 1.15, 1.19, 1.19, 1.18 and 1.07 eV for **1B**, **2B** and **1S**–**5S**, respectively. The HOMO levels were estimated by a comparison with the ionization potential of ferrocene, which has been determined to be 4.8 eV. A single reductive wave was observed for **1S**–**5S** in the range from −1.1 to −1.3 eV. The E_{red} of **1B** and **2B** were estimated by the 0–0 absorption energies in their UV spectra, which were estimated from the interception of the absorption and emission spectra. The E_{red} of **2S**, **3S** and **4S** are higher than that of **1B**, **2B** and **1S** for the existence of electron-accepting moiety such as cyano or oxadiazol substituents. The relatively high E_{red} and the observed reversible reductive process suggest that **2S**, **3S**, **4S** are favorable for electron injection, which enable them to be used as host emitter and electron transporter at the same time [38–40].

One type of device was made with configurations of ITO/NPB/maleimide/TPBI/LiF:Al. In the device, NPB worked as hole transporter (HT), while TPBI as an electron transporter. The EL spectrums and current–voltage–luminance (*I*–*V*–*L*) characteristics are shown in Figs. 7 and 8. The maximum EL apex was 640 nm for **1S**, which was red shifted about 30 nm com-

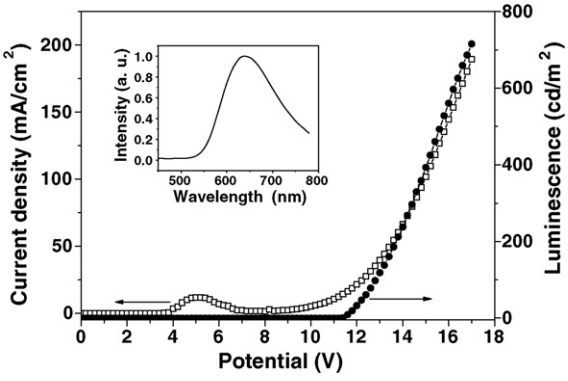

Fig. 7. EL spectrum and current density (*J*)–voltage (*V*)–brightness (*B*) characteristics of the device of **1S**.

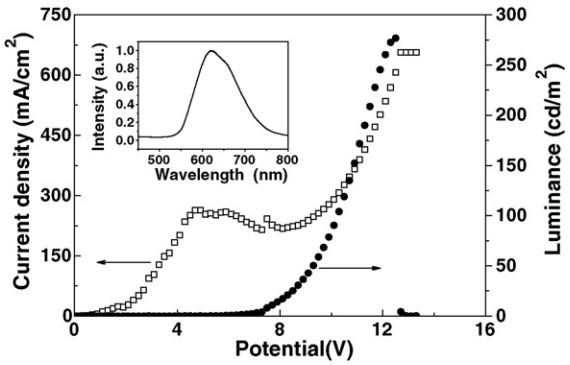

Fig. 8. EL spectrum and current density (J)–voltage (V)–brightness (B) characteristics of the device of **1B**.

pared with its photoluminescence (PL) spectrum in solid state. Similar phenomenon has been observed in NPAFN, which is a high-performance non-dopant type red emitting materials. Such difference between the maximum apex of PL and EL indicated that there is certain kind of aggregation formation providing charge-trapped sites with lower energy [27]. From the single crystal of **1S** we can speculate that this kind of aggregation formation would be the *J*-aggregation. The further experiments are in progressing. The maximum intensity of EL reached 715 and 276 cd m^{-2} for the devices made with compounds **1S** and **1B**, respectively. The maximum external quantum efficiencies were 0.24% (or 0.39 cd A^{-1}) for compound **1S** and 0.035% (or 0.057 cd A^{-1}) for **1B**, respectively.

The turn-on voltage for **1S** is 11.4 V, dramatically higher than other similar compounds reported in ref. [8]. The high turn-on voltage induces the low current density, and then reduces the luminescence intensity and debases the OLED performance enormously. Considering its wonderful luminescence property in solid state and high T_g, it must be a good candidate for non-doped red OLED. The EL devices are being optimized. In view of the reproducibility of the optimum doping level that requires careful manufacture control, OLEDs based on non-doped host emitters can simplify the manufacture consumedly. Though the performances of these new non-doped red organic light-emitting materials are not as good as conventional doped ones now, they are more promising in mass production. The optimal EL performances of the compounds are being done in progress. In this paper, we focus on the syntheses and spectral properties of the non-doped red organic light-emitters.

4. Conclusion

We have synthesized a new series of bisindolemaleimide derivatives. The absorption and fluorescence properties of these compounds were investigated in solution and solid state. By attaching different substituents on the fluorophores skeleton, a high solid-state emission red BIM derivative **1S** was developed. The aggregation configuration has been elucidated by means of X-ray crystallographic analyses. Owe to its special "pyramid mimetic" configuration, **1S** is endowed with high emission and T_g. **1B** and **1S** were successfully utilized in non-doping host red EL device. The brightness reaches 393 cd m^{-2} at 100 mA cm^{-2} for **1S**. By introducing oxadiazol or cyano groups to the bisindolemaleimide, the electron transport capability was improved and **2S**, **3S** and **4S** might be used as host emitter and electron transporting materials at the same time.

Supplementary material

Electronic supplementary information (ESI) available: X-ray structural data for compound **1S** (CCDC 611250) and compound **5S** (CCDC 611251). See http://dx.doi.org/.

Acknowledgements

Authors acknowledge the support by NSFC/China (90401026), National Basic Research 973 Program (2006CB-806200) and Scientific Committee of Shanghai.

Appendix A. Supplementary data

Supplementary data associated with this article can be found, in the online version, at doi:10.1016/j.jphotochem.2007.04.030.

References

[1] Y. Ooyama, T. Okamoto, T. Yamaguchi, T. Suzuki, A. Hayashi, K. Yoshida, Chem. Eur. J. 12 (2006) 7627.
[2] H.C. Yeh, W.C. Wu, Y.S. Wen, D.C. Dai, J.K. Wang, C.T. Chen, J. Org. Chem. 69 (2004) 6455.
[3] Y. Mizobe, N. Tohnai, M. Miyata, Y. Hasegawa, Chem. Commun. (2005) 1839.
[4] V. de Halleux, J.P. Calbert, P. Brocorens, J. Cornil, J.P. Declercq, J.L. Brédas, Y. Geerts, Adv. Funct. Mater. 14 (2004) 649.
[5] C.W. Tang, S.A. VansSlyke, Appl. Phys. Lett. 51 (1987) 913.
[6] C.L. Chiang, M.F. Wu, D.C. Dai, Y.S. Wen, J.K. Wang, C.T. Chen, Adv. Funct. Mater. 15 (2005) 231.
[7] C.T. Chen, Chem. Mater. 16 (2004) 4389.
[8] T.S. Yeh, T.J. Chow, S.H. Tsai, C.W. Chiu, C.X. Zhao, Chem. Mater. 18 (2006) 832.
[9] A. Dreuw, J. Plöner, L. Lorenz, J. Wachtveitl, J.E. Djanhan, J. Brüning, T. Metz, M. Bolte, M.U. Schmidt, Angew. Chem. Int. Ed. 44 (2005) 7783.
[10] Y. Ooyama, K. Yoshida, New J. Chem. 29 (2005) 1204.
[11] S. Mizukami, H. Houjou, K. Sugaya, E. Koyama, H. Tokuhisa, T. Sasaki, M. Kanesato, Chem. Mater. 17 (2005) 50.
[12] K. Yoshida, K. Uwada, H. Kumaoka, L. Bu, S. Watanabe, Chem. Lett. (2001) 808.
[13] Y. Ooyama, T. Nakamura, K. Yoshida, New J. Chem. 29 (2005) 447.
[14] J.L. Scott, T. Yamada, K. Tanaka, New J. Chem. 28 (2004) 447.
[15] Y. Sonoda, Y. Kawanishi, T. Ikeda, M. Goto, S. Hayashi, N. Tanigaki, K. Yase, J. Phys. Chem. B 107 (2003) 3376.
[16] K. Hirano, S. Minakata, M. Komatsu, Chem. Lett. (2001) 8.
[17] Z. Fei, N. Kocher, C.J. Mohrschladt, H. Ihmels, D. Stalke, Angew. Chem. Int. Ed. 42 (2003) 783.
[18] E. Tedesco, F.D. Sala, L. Favaretto, G. Barbarella, D. Albesa-Jove, D. Pisignano, G. Gigli, R. Cingolani, K.D.M. Harris, J. Am. Chem. Soc. 125 (2003) 12277.
[19] C.L. Donley, J. Zaumseil, J.W. Andreasen, M.M. Nielsen, H. Sirringhaus, R.H. Friend, J.S. Kim, J. Am. Chem. Soc. 127 (2005) 12890.
[20] L. Antolini, E. Tedesco, G. Barbarella, L. Favaretto, G. Sotgiu, M. Zambianchi, D. Casarini, G. Gigli, R. Cingolani, J. Am. Chem. Soc. 122 (2000) 9006.
[21] G. Barbarella, L. Favaretto, G. Sotgiu, L. Antolini, G. Gigli, R. Cingolani, A. Bongini, Chem. Mater. 13 (2001) 4112.

[22] C.C. Chao, M.K. Leung, Y.O. Su, K.Y. Chiu, T.H. Lin, S.J. Shieh, S.C. Lin, J. Org. Chem. 70 (2005) 4323.
[23] T.H. Liu, C.Y. Iou, C.H. Chen, Appl. Phys. Lett. 83 (2003) 5241.
[24] K.R.J. Thomas, J.T. Lin, Y.T. Tao, C.H. Chuen, Adv. Mater. 14 (2002) 822.
[25] W.C. Wu, H.C. Yeh, L.H. Chan, C.T. Chen, Adv. Mater. 14 (2002) 1072.
[26] C.T. Chen, Y. Wei, J.S. Lin, M.V.R.K. Moturu, W.S. Chao, Y.T. Tao, C.H. Chien, J. Am. Chem. Soc. 128 (2006) 10992.
[27] Y. Qiu, P. Wei, D.Q. Zhang, J. Qiao, L. Duan, Y.K. Li, Y.D. Gao, L.D. Wang, Adv. Mater. 18 (2006) 1607.
[28] H.C. Yeh, S.J. Yeh, C.T. Chen, Chem. Commun. (2003) 2632.
[29] S.Y. Chen, X.J. Xu, Y.Q. Liu, G. Yu, X.B. Sun, W.F. Qiu, Y.Q. Ma, D.B. Zhu, Adv. Funct. Mater. 15 (2005) 1541.
[30] C.Q. Ma, B.X. Zhang, Z. Liang, P.H. Xie, X.S. Wang, B.W. Zhang, Y. Cao, X.Y. Jiang, Z.L. Zhang, J. Mater. Chem. 12 (2002) 1671.
[31] C.W. Chiu, T.J. Chow, C.H. Chuen, H.M. Lin, Y.T. Tao, Chem. Mater. 15 (2003) 4527.
[32] T.J. Chow, S.H. Tsai, C.W. Chiu, T.S. Yeh, Synth. Met. 149 (2005) 59.
[33] S. Alex, U. Santhosh, S. Das, J. Photochem. Photobiol. A: Chem. 172 (2005) 63.
[34] J. Cornil, D. Beljonne, J.P. Calbert, J.L. Brédas, Adv. Mater. 13 (2001) 1053.
[35] M. Irie, Chem. Rev. 100 (2000) 1685.
[36] X. Li, H. Tian, Tetrahedron Lett. 46 (2005) 5409.
[37] T. Kaieda, S. Kobatake, H. Miyasaka, M. Urakami, N. Wai, Y. Agata, A. Taya, M. Irie, J. Am. Chem. Soc. 124 (2002) 2015.
[38] N. Tamoto, C. Adachi, K. Nagai, Chem. Mater. 9 (1997) 1077.
[39] Z.H. Li, M.S. Wong, H. Fukutani, Y. Tao, Chem. Mater. 17 (2005) 5032.
[40] W.H. Zhu, M. Hu, R. Yao, H. Tian, J. Photochem. Photobiol. A: Chem. 154 (2003) 169.